ENERGETICS AT MASS 92, 94 and 96

and

A MAGNETIC FIELD REGULATOR

A MASS SPECTROGRAPHIC STUDY OF THE ENERGETICS AT MASS NUMBERS 92, 94 and 96

and

A PROPOSED DESIGN OF A PROTON RESONANCE MAGNETIC FIELD REGULATOR

By

James Stephen Geiger, B. Sc.

A Thesis

Submitted to the Faculty of Arts and Science

in Partial Fulfilment of the Requirements

for the Degree

Master of Science

McMaster University

September 1952

MASTER OF SCIENCE (1952)
(Physics)

McMASTER UNIVERSITY
Hamilton, Ontario

TITLE: A Mass Spectrographic Study of the Energetics at Mass Numbers 92, 94 and 96

and

A Proposed Design of a Proton Resonance Magnetic Field Regulator

AUTHOR: James Stephen Geiger, B. Sc. (McMaster University)

SUPERVISOR: Professor H. E. Duckworth

NUMBER OF PAGES: 33

SCOPE AND CONTENTS:

PART A - Mass spectrographic measurements are reported of the following mass differences: $1/2W^{184} - Zr^{92}$, $1/2W^{184} - Mo^{92}$, $1/2\ Os^{188} - Zr^{94}$, $1/2\ Os^{188} - Mo^{94}$, $1/2\ Os^{192} - Zr^{96}$, $1/2\ Os^{192} - Mo^{96}$, and $1/2\ Os^{192} - Ru^{96}$. These results are used to check and supplement existing transmutation and disintegration data in the region of the $Zr^{92} - Mo^{92}$ and $Zr^{94} - Mo^{94}$ isobaric pairs and the $Zr^{96} - Mo^{96} - Ru^{96}$ isobaric triplet.

PART B - The operation of proton resonance controlled magnetic field strength regulators is outlined. The results of tests on an experimental model regulator are given along with a proposed regulator design based on these tests.

ACKNOWLEDGEMENTS

I wish to thank my supervisor, Professor H. E. Duckworth, for his kind assistance and direction in this work, and Professor A. B. McLay for the interest he has shown in the preparation of this thesis.

I have greatly enjoyed my association with Mr. J. T. Kerr in this work and I should like to express my thanks to Mr. J. G. Bayley of the Chalk River Laboratories for a most helpful discussion of proton resonance regulators.

I am most grateful for the financial assistance of the Research Council of Ontario which has made it possible for me to undertake graduate studies.

TABLE OF CONTENTS

PART A

A MASS SPECTROGRAPHIC STUDY

PART B

A PROPOSED MAGNETIC FIELD REGULATOR

LIST OF ILLUSTRATIONS

PART A

PART B

TABLES

PART A

A MASS SPECTROGRAPHIC STUDY

INTRODUCTION

A description is given of the mass spectrographic determination of the Zr^{92}- Mo^{92}, Zr^{94}- Mo^{94}, Zr^{96}- Mo^{96} and Ru^{96}- Mo^{96} mass differences. The information so obtained is used in checking the correctness of certain transmutation and disintegration data and in estimating the energy available for unobserved reactions.

EXPERIMENTAL

The measurements herein reported were made by the doublet method using our large Dempster-type mass spectrograph[1]. The ion source was a high frequency spark. One electrode of the spark consisted of a thin-walled nickel tube which was packed with the pair of elements under study at the time. The mass differences obtained are shown in Table I. Exposure times ranged from 5-10 minutes. Table 1 is on page 11.

The Zr^{92}- Mo^{92} Stable Isobaric Pair

Nb^{92} has been found to decay to both Zr^{92} and Mo^{92}. There is a 0.93 Mev. gamma ray in the K-capture branch[2] leading to Zr^{92}, which represents all but 0.05% of the transitions while the end point of the negatron group leading to Mo^{92} has been reported[3][4] to be 1.38 Mev.

It is possible to compute the energy available for the K-capture decay in two ways using existing transmutation data. The first calculation is based on the Nb^{93} (γ,n) threshold[5] of 8.7 Mev, a Q[6] of 4.35

Mev for the Zr^{92}(d,p) reaction, and values of 0.19[7] and 0.06[8] Mev for the end point of the Zr^{93} negatrons, viz:

$$Nb^{93} - Nb^{92} = 0.99964 \pm 21 \text{ AMU}$$
$$Zr^{93} - Zr^{92} = 1.00193 \pm 21 \text{ AMU}$$
$$Zr^{93} - Nb^{93} = 0.00013 \pm 7 \text{ AMU}$$
$$\text{therefore, } Nb^{92} - Zr^{92} = 0.00216 \pm 30 \text{ AMU}$$
$$= 2.0 \pm 0.3 \text{ Mev}$$

The second is based on 2.5 Mev for the $Zr^{92}(p,n)Nb^{92}$ threshold,[9] and gives the value $Nb^{92} - Zr^{92} = 1.7 - 0.2$ Mev. These two figures are in satisfactory agreement and appear consistent with a K-capture branch containing a 0.93 - Mev gamma ray. We are assuming a value of 1.8 ± 0.2 Mev for the $Nb^{92} - Zr^{92}$ mass difference.

It is likewise possible to compute a value for the $Nb^{92} - Mo^{92}$ decay energy. The pertinent data are 8.7 ± 0.2 Mev[5] for the Nb^{93}(,n) threshold, 6.08 ± 0.2 Mev[6] for the of the Mo^{92}(d,p) reaction, 3.7 ± 0.2 Mev[9] for the $Nb^{93}(p,n)Mo^{93m}$(6.75 hr) threshold, and 2.5 - 2.7 Mev[10,11] for the Mo^{93m} Mo^{93} transition. Thus,

$$Nb^{93} - Nb^{92} = 0.99964 \pm 21 \text{ AMU}$$
$$Mo^{93} - Mo^{92} = 1.00005 \pm 21 \text{ AMU}$$
$$Mo^{93m} - Nb^{93} = 0.00309 \pm 21 \text{ AMU}$$
$$Mo^{93m} - Mo^{93} = 0.00279 \pm 10 \text{ AMU}$$
$$\text{therefore, } Nb^{92} - Mo^{92} = 0.00011 \pm 38 \text{ AMU}$$
$$= 0.1 \pm 0.4 \text{ Mev}$$

It appears from this result that the 1.38-Mev beta ray is not a transition from the ground state of Nb^{92} to the ground state of Mo^{92}.

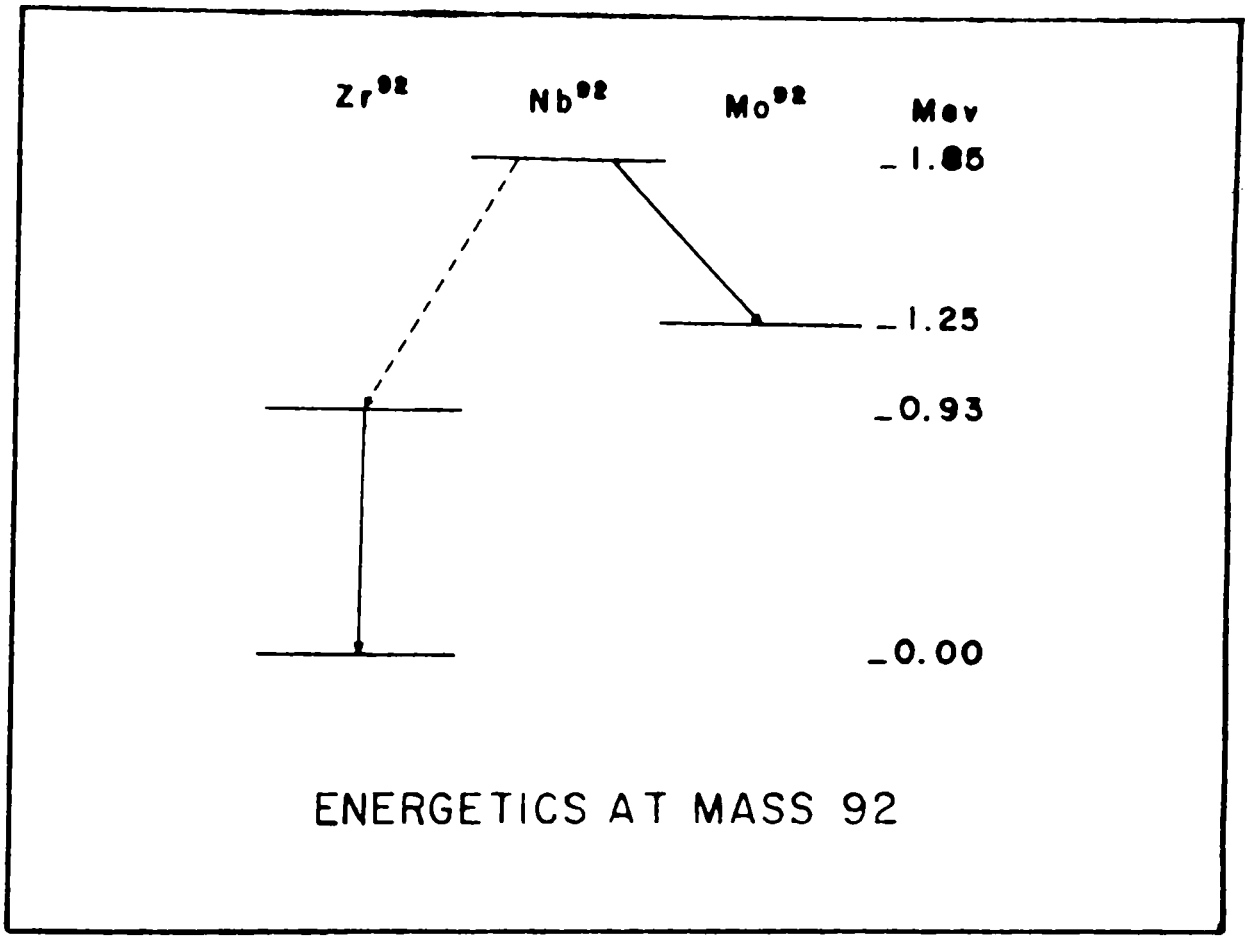

ENERGETICS AT MASS 92

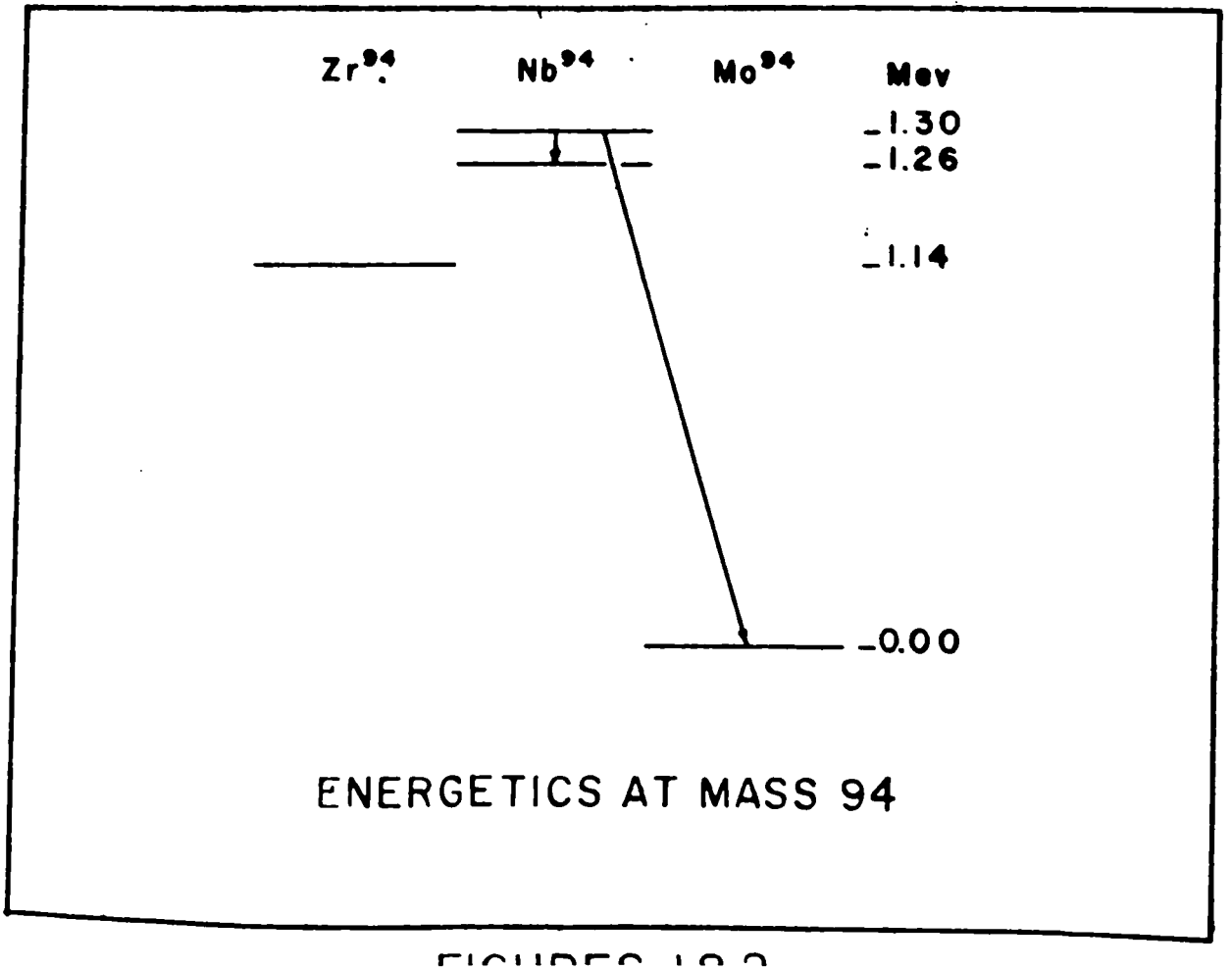

ENERGETICS AT MASS 94

FIGURES 12.2

These calculations indicate that the $Mo^{92} - Zr^{92}$ mass difference is $(1.8 \pm 0.2) - (0.1 \pm 0.4) = 1.7 \pm 0.4$ Mev. From our experiments, as seen from Table I, this difference has been found to be 1.25 ± 0.25 Mev. These results are in satisfactory agreement, especially when one considers that the computed values are based on a chain of several measurements, each of which is subject to an error of 0.1 - 0.2 Mev. The energy relationships between Zr^{92}, Nb^{92} and Nb^{92} are shown in Fig. 1.

The $Zr^{94} - Mo^{94}$ Isobaric Pair

The state of knowledge of Nb^{94} is shown in figure 2[10]. It is not possible to compute the $Zr^{94} - Mo^{94}$ mass difference from disintegration or transmutation data. From Table I it is seen that the measured $Zr^{94} - Mo^{94}$ mass difference is 1.14 ± 0.2 Mev. This leaves 0.12 Mev of energy available for the K-capture mode of decay from the ground state of Nb^{94}, a figure which explains the lack of success[11] with which experiments to detect it have met.

The $Zr^{96} - Mo^{96} - Ru^{96}$ Isobaric Triplet

Some knowledge of the $Zr^{96} - Mo^{96}$ mass difference may be got from the $Zr^{96}(p,n)$ threshold plus the various studies of the decay scheme of Nb^{96}.

Regarding the $Zr^{96}(p,n)$ threshold, this has been found by Blaser

et al[9] to be 2.6 Mev. When this is compared to 2.5 Mev. for the Zr^{92}(p,n) threshold, obtained in the same laboratory, it is difficult to believe that both can be correct. One would expect the figure for Zr^{96} to be much lower than that for Zr^{92}. The latter has been seen above to be consistent with the other data at mass number 92. Consequently, we are assuming that the reported Zr^{96}(p,n) value is in error.

Concerning the Nb^{96}- Mo^{96} decay, three values have been reported for the total decay energy: these are 3.14 Mev[12], 3.16 Mev[2], and 1.98 Mev[13]. Our value for the Zr^{96}- Mo^{96} mass difference is 3.4 ± 0.3 Mev, which is larger than any of the figures for the Nb^{96}- Mo^{96} difference. This implies either that there is more energy in the Nb^{96} decay than is presently realized, or that Zr^{96} is unstable against beta-decay to Nb^{96}. The former possibility does not seem very likely since two recent independent measurements agree closely on the total decay energy for Nb^{96}. The second possibility, which is the more likely, is analagous to the case of Ca^{48} which does not decay to Se^{48}, although energetically possible, because of the large spin change involved[14]. Further, it is interesting to note that McCarthy[15] has obtained preliminary evidence for an activity of 3.3 - 4.3 Mev. in Zr^{96}. This activity, if authentic, would represent the double beta-decay of Zr^{96} to Mo^{96}.

Turning now the the Ru^{96}- Mo^{96} pair, it is known that Tc^{96} decays to Mo^{96} by K-capture and possibly to Ru^{96} by negatron emission. In the former case, 2.73 Mev[16] of gamma rays follow the K-capture event, while the negatron group, if it exists, has an end point of $\sim$ 0.8 Mev[17][18].

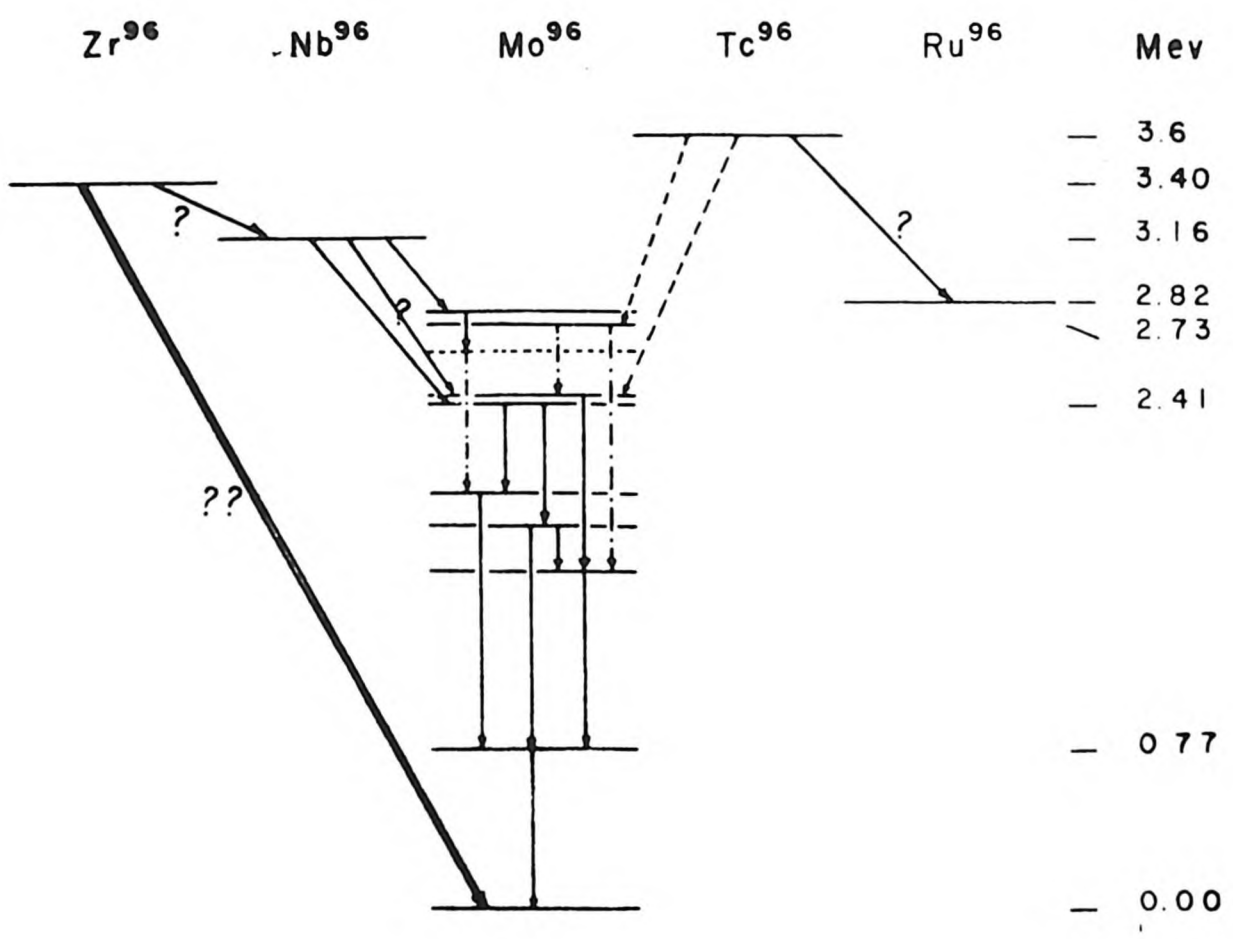

ENERGETICS AT MASS 96

FIGURE 3

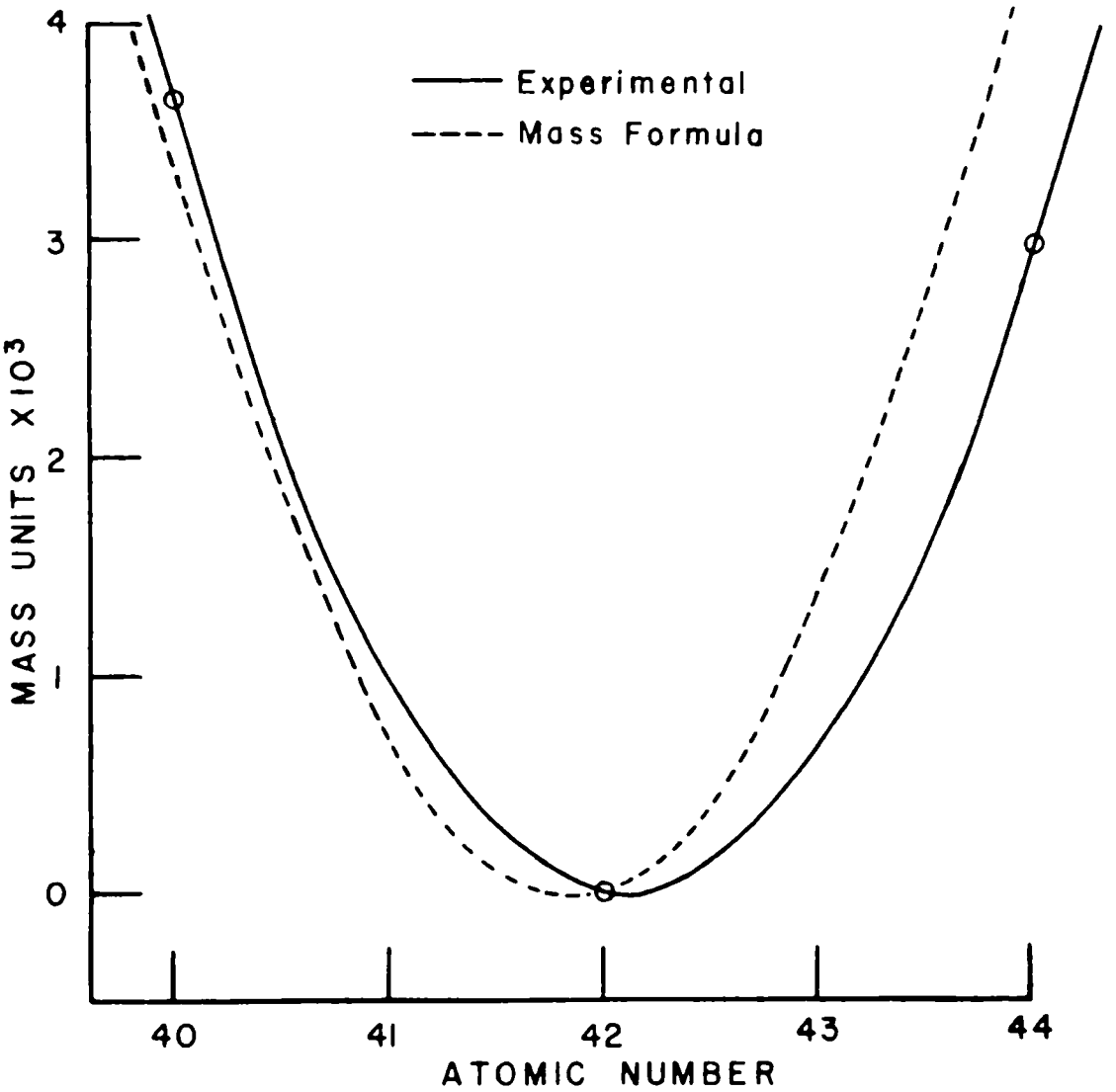

THE EXPERIMENTAL AND THEORETICAL PARABOLAE AT MASS 96.

ASSUMING A FORM $({}_{Z}M^{A} - {}_{Z_0}M^{A}) = \frac{B}{2}(Z - Z_0)^2$, THE PARAMETERS IN THE EXPERIMENTAL CASE ARE $B = 1.55$; $Z_0 = 42.1$ AND IN THE THEORETICAL CASE ARE $B = 1.94$; $Z = 41.8$

FIGURE 4

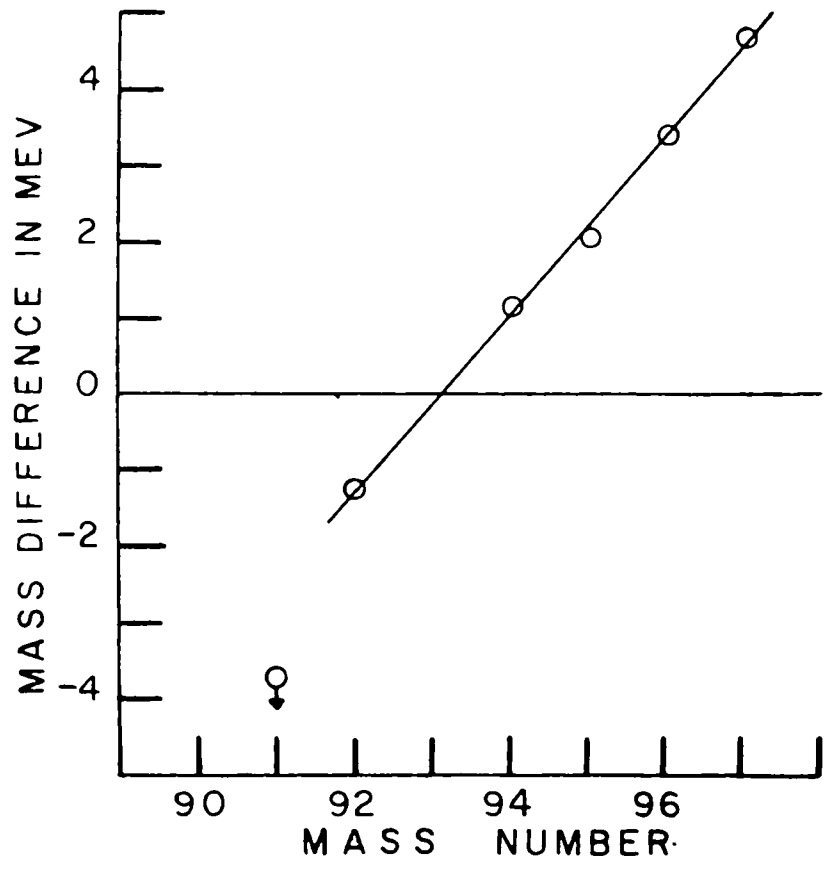

A PLOT OF THE ISOBARIC ZR - MO
MASS DIFFERENCES VS. MASS NUMBER

FIGURE 5

Both these data are consistent with our measurement of 2.8 ± 0.2 Mev. for the Ru^{96} - Mo^{96} mass difference. Figure 3 shows the level schemes at mass number 96.

It is interesting to use our values for the Zr^{96} - Mo^{96} and Ru^{96} - Mo^{96} mass differences to construct at mass 96 the even-even parabola, which is predicted by the semi-empirical mass formula. This is done in figure 4, where it is compared to the parabola resulting from the use of the computed masses (with suitable vertical displacement) of Metropolis and Reitwiesner[19].

The experimental parabola is seen to be wider than the predicted one. This also follows from the experiments of the Columbia group[20] who have found the sides of the valley of stability at constant Z (for Z = 32 and Z = 34) to be less steep than given by the computed masses.

Discussion of the Mo-Zr Mass Differences

Some Mo-Zr mass differences at odd mass numbers have been found by studying the decay schemes involved, viz: $Mo^{91} - Zr^{91} \geq 2.9$ Mev[21], $Zr^{95} - Mo^{95} = 2.04$ Mev[22], and $Zr^{97} - Mo^{97} = 4.59$ Mev.[23]. In figure 5 these values are plotted together with our $Mo^{92} - Zr^{92}$, $Zr^{94} - Mo^{94}$ and $Zr^{96} - Mo^{96}$ results. The mass difference appears to be a linear function of the mass number from mass 92 to 96.

The widespread existence of linear relationships of this type has been pointed out to us by Dr. Katharine Way and Miss Marion Wood, and will, we understand, be described in detail by them in a future publication. The semi-empirical mass formula also predicts an approximately linear curve. We, therefore, regard Figure 5 as an indication of the general

correctness of our results. The departure of the point at mass number 91 from the straight line curve is adequately explained by the extra energy involved in the Mo^{91}-Nb^{91} transition, owing to the ease with which Mo^{91} is transformed into the 50 neutron configuration, Nb^{91}.

These results indicate that Zr^{93} and Mo^{93} are practically equal in mass. This is compatible with the fact that Zr^{93} has a half-life of $> 4 \times 10^6$ years and Mo^{93} decays by K-capture with presumably a long life time.

Summary

The results of this investigation are summarized as follows:

(a) The reported value of 3.7 Mev for the Nb^{93} (p,n) threshold appears to be incorrect.

(b) The reported value, 1.38 Mev, for the end point of the negatron group leading to Mo^{92} is not consistent with other related data which suggest that this end point lies in the region of 0.5 Mev.

(c) An energy of 0.12 Mev is available for the K-capture decay of Nb^{94}, a figure which explains the lack of success with which experiments to detect it have met.

(d) The Zr^{96}(p,n) threshold of 2.6 Mev reported by Blaser is incorrect.

(e) It is probable that the decay of Zr^{96} to Nb^{96} is energetically possible.

(f) The Mo - Zr isobaric mass difference appears to be a linear function of the mass number from mass 92 to 96.

Table I - Mass Spectrographic Mass Differences

Nuclides	Mass Difference (mMU)	Previous Measurements
$_{74}W^{184} - Zr^{92}$	69.79 ± 0.14	74.1 ± 1.8[a] 69.3 ± 0.4[b]
$_{74}W^{184} - Mo^{92}$	68.45 ± 0.22	———
$_{76}Os^{188} - Zr^{94}$	71.34 ± 0.12	———
$_{76}Os^{188} - Mo^{94}$	72.56 ± 0.16	73.1 ± 2.8[a]
$_{76}Os^{192} - Zr^{96}$	71.83 ± 0.24	———
$_{76}Os^{192} - Mo^{96}$	75.46 ± 0.14	72.8 ± 2.9[a]
$_{76}Os^{192} - Ru^{96}$	72.44 ± 0.17	75.9 ± 1.9[c] 73.4 ± 1.3[c]

a. A. J. Dempster, Phys. Rev. 53, 64(1938)

b. H. E. Duckworth, C. L. Kegley, J. M. Olson and G. S. Stanford, Phys. Rev. 83, 1114-1117(1951)

c. A. C. Graves, Phys. Rev. 55, 863(1939)

PART B

A PROPOSED MAGNETIC FIELD REGULATOR

INTRODUCTION

A large, semi-circular, magnetic momentum analyser is under construction in this laboratory for use in a mass spectrometer of high resolution. This analyser is comprised of twenty-eight C-magnets shaped to form a semi-circle of nine foot radius when placed side by side. In such an analyser, assuming a homogeneous magnetic field, the mass m of the ions of given energy E which describe a circle of radius R is proportional to the square of the magnetic field strength H, as seen in equation (1).

$$m = \frac{e^2 R^2}{2E} \cdot H^2 \qquad (1)$$

The completed mass spectrometer is to have a mass resolution, $\frac{dm}{m}$, of 1 part in 100,000. It is therefore necessary that the magnetic field strength be stabilized to 1 part in 200,000. This follows from equation (2).

$$\frac{dm}{m} = 2\frac{dH}{H} \qquad (2)$$

Various methods can be used for stabilizing a magnetic field. Degenerative magnet current regulators do not regulate the magnetic field strength to better than one part in several thousand[24] since the magnetic field strength is a function of the magnet geometry and the permeability of the iron (both of which vary with temperature) as well as of the magnet current. Furthermore these regulators do not provide either an absolute or a relative measure of the magnetic field strength.

Recently nuclear resonance techniques[25][26][27] have been used to both measure and stabilize magnetic field strength. Using proton

resonance it is possible to obtain magnetic field strength stabilization ratios of 10^5 to 10^6 and to make absolute field strength measurements to accuracies approaching 0.0025 percent[24]. This is the accuracy with which the absolute value of the proton gyromagnetic ratio has been measured by Thomas, Driscoll and Hipple[28]. The stabilization ratio attainable is limited by the instability of the radio-frequency oscillator which must be used and by the width of the proton resonance, which depends in turn on the homogeniety of the magnetic field in the region of the sample and on the nature of the material used as the sample[27]. This method has been chosen for use with the large analyser.

The Proton Resonance Phenomenon

Protons have a nuclear spin $I = \frac{1}{2}$ and a nuclear magnetic moment μ_p. In the presence of a magnetic field of strength H_o the nuclear spin vector of the proton can have only one of two possible orientations with respect to that field. The two energy states corresponding to these two possible spin vector orientations differ in their energy by an amount Δw where

$$\Delta w = \frac{\mu_p H_o}{I} = h\nu \qquad (3)$$

When thermal equilibrium exists in a proton sample immersed in a magnetic field H_o, there is, at ordinary temperatures, a slight surplus of protons in the lower of the two energy states. If a weak radio-frequency field of frequency ν, given by equation (3), is present in the region of the proton sample transitions are induced between these two energy levels. This results in a net absorption of energy from the radio-frequency field as long as there remains an excess of protons in the lower of the two energy states.

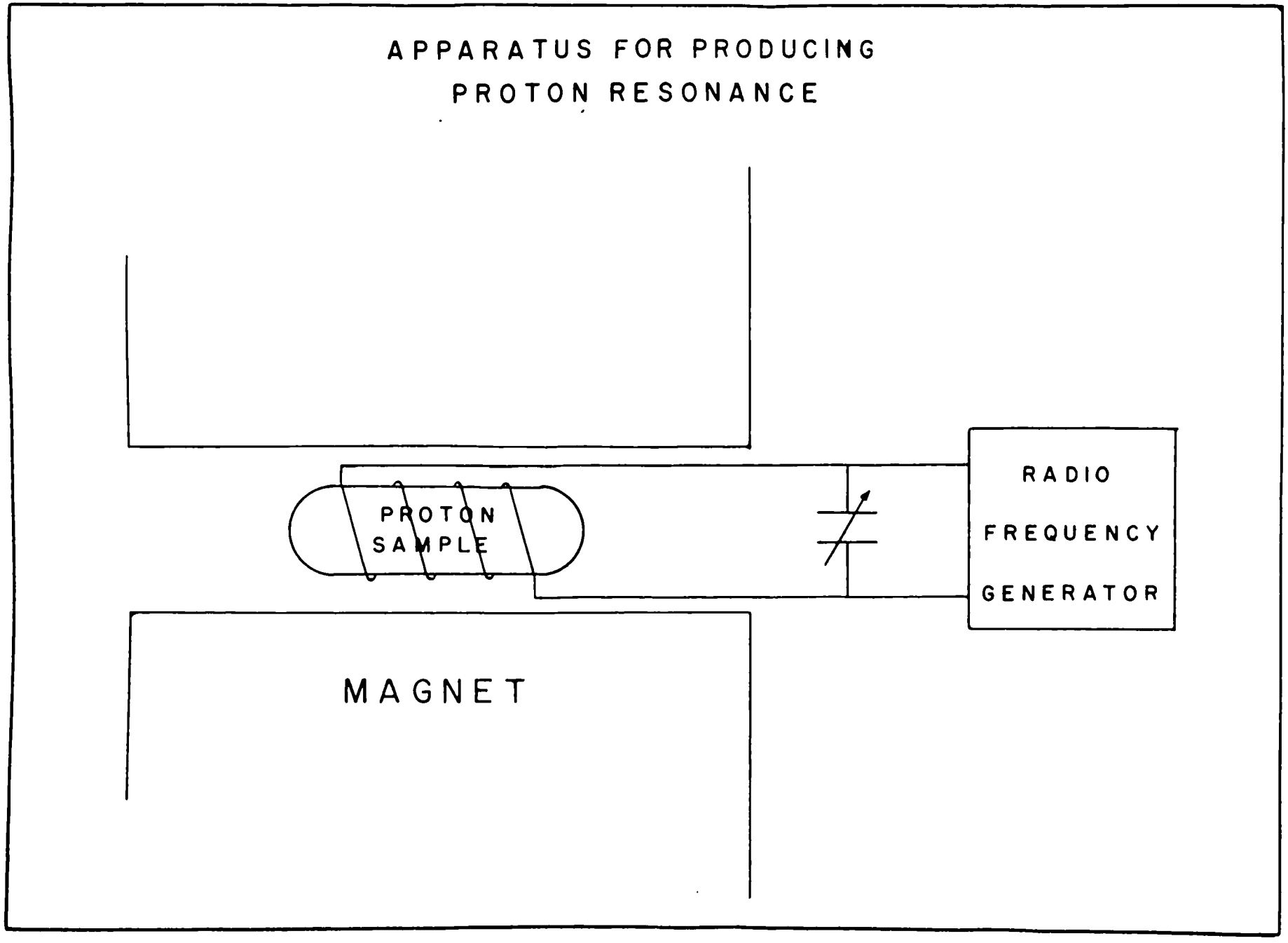
APPARATUS FOR PRODUCING
PROTON RESONANCE
PROTON
SAMPLE
RADIO
FREQUENCY
GENERATOR
MAGNET

FIGURE 6

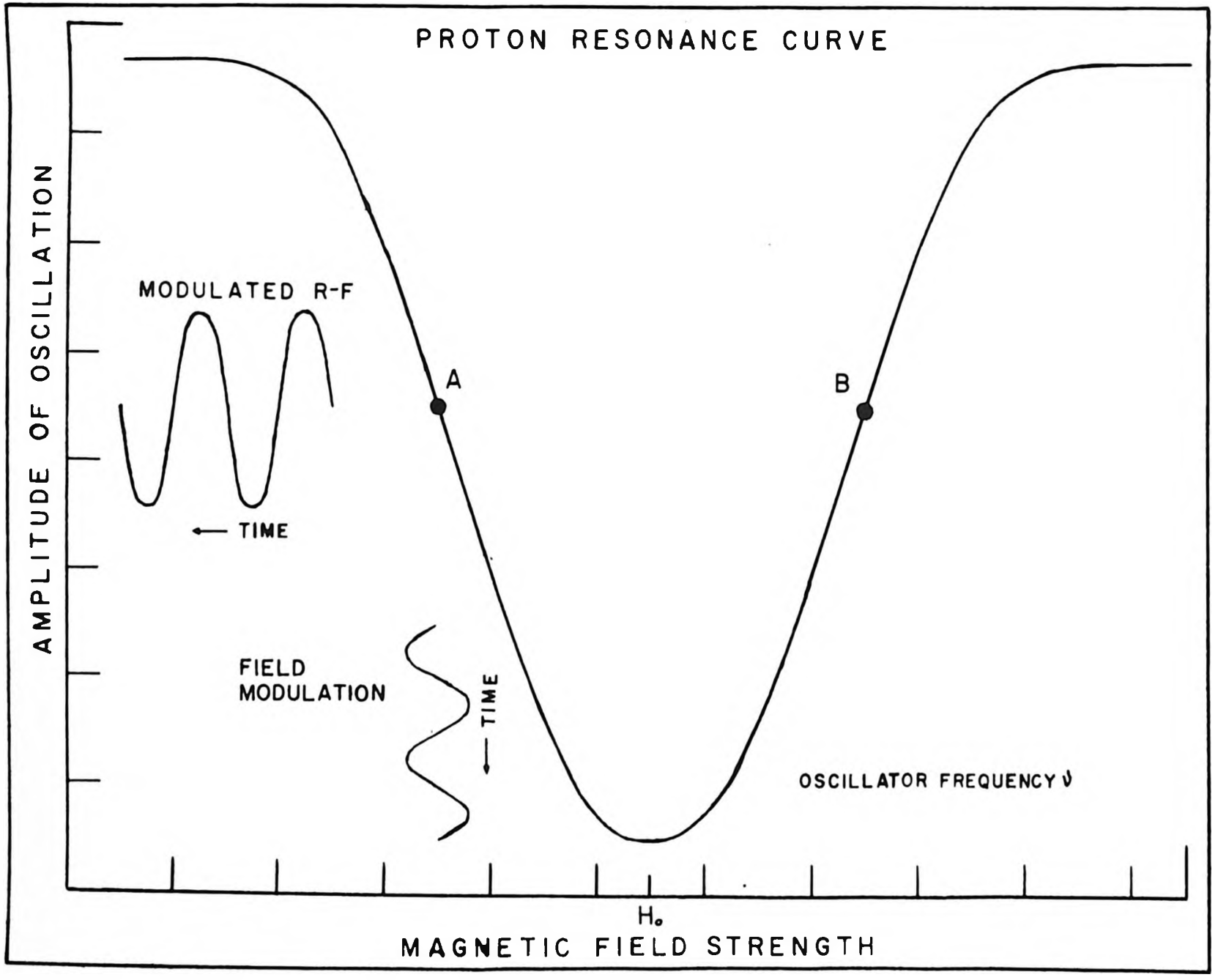
PROTON RESONANCE CURVE
AMPLITUDE OF OSCILLATION
MODULATED R-F
TIME
A
B
FIELD
MODULATION
TIME
OSCILLATOR FREQUENCY ν
H₀
MAGNETIC FIELD STRENGTH

FIGURE 7

It is found that energy is absorbed from a radio-frequency field of frequency ν not only at a magnetic field strength H_0 but at all values of magnetic field strength in the interval $H_0 \pm \Delta H$. The magnitude of ΔH is governed by properties of the material being used as the proton sample and by the inhomogeniety of the magnetic field over the region occupied by the sample[27].

The Detection of Nuclear Resonance Absorption

A simple apparatus for producing proton resonance is shown in figure 6. When the condition of equation (3) prevails energy is absorbed from the r-f field. This absorption of energy results in a decrease in the Q of the parallel resonant circuit and a decrease in its impedance. Detection of the nuclear resonance therefore involves detecting a small change in the large impedence of the parallel tuned circuit. Radio-frequency bridge circuits have been used for this purpose[27]. However such circuits require critical adjustment and are not readily tuneable. Various regenerative[29][30][31][32][33][28] and supor-regenerative oscillators[29][34] which can be readily tuned have been used to detect nuclear resonance signals. When oscillations are at a low level in these circuits their magnitude is extremely sensitive to small changes in the impedance of the resonant circuit. Figure 7 gives a qualitative representation of the variation of the amplitude of oscillation in these circuits in the region of the proton resonance.

It is customary to modulate the magnetic field or the r-f frequency at an audio rate. In the region of resonance this results in an audio-frequency amplitude modulation of the r-f oscillations (as described in the next section) of a form governed by the shape of the proton resonance peak. By using a suitable detector and audio amplifier the proton reson-

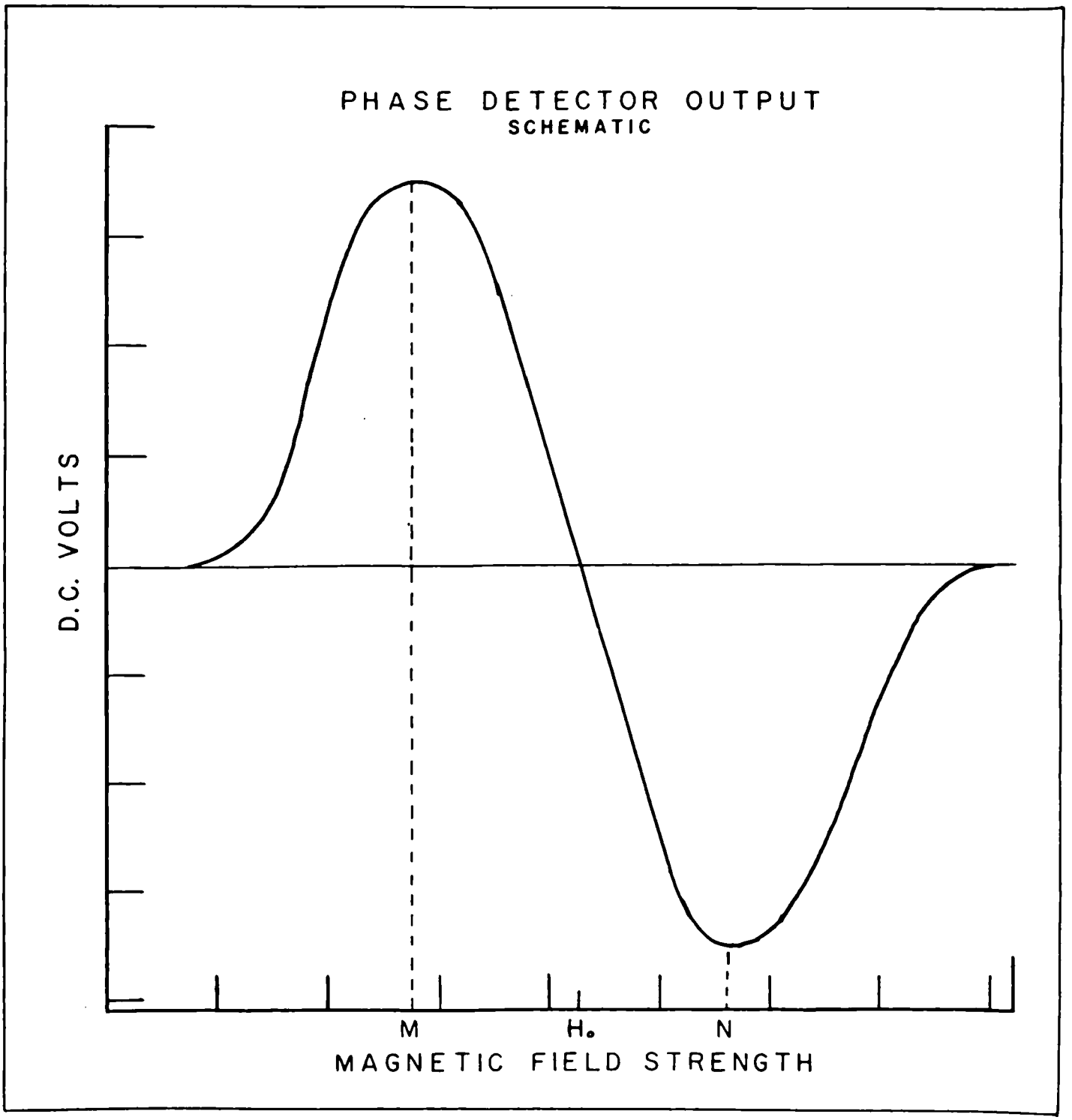
PHASE DETECTOR OUTPUT
SCHEMATIC
D.C. VOLTS
M
H₀
N
MAGNETIC FIELD STRENGTH

FIGURE 8

ance absorption peak can be observed on an oscilloscope.

The Theory of the Operation of a Proton Resonance Absorption Magnetic Field Discriminator

A curve illustrating the variation of the amplitude of radio-frequency oscillation with magnetic field strength in the region of resonance is given in figure 7. Pictured on this curve are two points A and B representing two values of the magnetic field strength in the region of resonance. If the magnetic field at A be modulated by a small sinusoidally varying field, of say 400 cycles, a 400 cycle amplitude modulation of the r-f oscillations results. The amplitude of this modulation is proportional to the slope of the proton resonance curve at A. If the magnetic field is shifted so that the field modulation is applied about the point B the resulting amplitude modulation of the r-f oscillations will have an amplitude proportional to the slope of the proton resonance curve at B but will be shifted in phase by 180° from its value at A.

If a suitable amplitude modulation detector and audio-frequency amplifier are used and the amplifier output is beat against the voltage producing the magnetic field modulation in a phase sensitive detector, a d.c. frequency-difference voltage will be produced. Providing that both the field modulation and amplifier output signals are 400 cycle sine waves, the value of this d.c. voltage will be a linear function of the amplitude of the detected signal, and its sign will be determined by the relative phase of the field modulation voltage and the detected signal. The output from the phase sensitive detector varies with the magnetic field strength in a manner similar to the derivative of the proton resonance absorption curve and is represented schematically in figure 8.

Since the proton resonance absorption curve has a continuously changing slope, a 400 cycle sine wave field modulation does not result in a 400 cycle sine wave amplitude modulation of the r-f oscillations. In order to obtain an output from the phase sensitive detector of the form shown in figure 8 it is necessary to pass the detected signal through a narrow band amplifier which amplifies only the 400 cycle sine wave component of the signal before feeding it into the phase sensitive detector. The properties of the curve in figure 8 in the region MN are suitable for regulating the magnet current since a positive or negative error voltage is obtained for a value of the field below or above resonance.

Design of Apparatus

(1) Introduction

Experiments have been performed which have led to the design of a proton resonance controlled magnetic field strength regulator. These experiments have been carried out using a rectangular yoked electromagnet whose gap width is 0.87 in. and whose pole faces measure 8 in. by 4 in. The magnet coil used was one of the twenty-eight identical coils constructed for use in the large momentum analyser now being built. The magnet current power supply used was the one designed for use with the large analyser and is described on page24.

(2) A Transitron Nuclear Resonance Detector

Our initial experiments to detect the proton resonance were made using a transitron, negative resistance oscillator circuit designed by Knoebel and Hahn[32]. This circuit uses frequency modulation rather than the more conventional field modulation. This unit was found to be extremely microphonic because of the effect of jarring on the motion of the vibrating

reed of the variable capacitor used to provide the frequency modulation. Such behaviour is not compatible with the use of the circuit in a magnetic field strength regulator of high stability. For this reason and on the advice of Mr. J. G. Bayley of Chalk River we switched to a detector circuit employing magnetic field modulation.

Using this latter type of detector circuit, we have constructed an experimental model field regulator and performed tests on the various circuits involved. The results of these tests are given in the following along with a proposed regulator design based on them. A block diagram of the proposed regulator is given in figure 9 and the schematic diagrams of the various circuits in figures 10,11,12,13,14,15 and 18. The field modulator and a regulated power supply have already been built while the probe, detector and preamplifier are now under construction.

(3) The Probe

The methods to be used for mounting and shielding the r-f coil containing the proton sample and for providing the magnetic field modulation in the proposed regulator are shown in figures 16 and 17. The design of the probe used in the experimental regulator differs only in detail from that given here. To provide field modulation a pair of coaxial, Helmholtz-like coils, each consisting of 50 turns of #32 formex wire are to be wound on a lucite form. An r-f coil of 3/8 in. diameter and $1\frac{1}{4}$ in. in length is to be mounted inside this lucite form, midway between the two coils and with its axis at right angles to theirs. This coil will be coupled to the oscillator circuit by 2 lengths of 1/16 in. brass rod which will be enclosed in a paraffin filled piece of 3 cm wave guide.

(4) The Proton Sample

In the experimental work ferric nitrate solutions of various concentrations were used as the sample since they gave rise to a relatively large resonance signal. A glass vial of such a size as to fit snugly inside the r-f coil of the probe served as a container. The glass vial to be used in the probe now under construction will be made from thin-walled glass tubing. The concentration of the ferric nitrate solution to be used as the sample will have to be determined by experiment[24][27].

(5) The Field Modulator

In order to make possible the use of a 390 cycle narrow band amplifier which was kindly made available to us by Dr. G. A. Miller, Chief of the Microwave Section of the Radio Laboratory of the National Research Council, we have chosen a 390 cycle field modulation frequency. Field modulation is provided by feeding the output from an audio oscillator into the pair of coaxial coils mounted in the probe.

The audio frequency oscillator shown in figure 12 is the Wien bridge type oscillator which Thomas has used[24] to supply the field modulating coils. The ganged-potentiometer R_{12} and R_{13} permits the oscillator frequency to be varied. Two individually controlled output voltages from the oscillator feed the single stage triode amplifiers which are transformer coupled to the modulating coils and the phase detector. A switching arrangement, shown in figure 13, is used which permits the oscillator output to be fed directly into the narrow band amplifier whose output is then fed into an oscilloscope. With these connections the oscillator can be adjusted to the 390 cycle frequency for which the amplifier has the maximum gain.

(6) A Push-Pull, Negative Resistance Oscillator Detector

The oscillator circuit shown in figure 10 has been described by Thomas[24] who has used a modified version of it in a magnetic field strength regulator. The coil containing the proton sample serves as the tank circuit inductor for the push-pull oscillator. A large capacitance is used to provide the grid leak bias in order to prevent the oscillator bias from fluctuating when amplitude modulation of the r-f current occurs at resonance. It was found that the noise level of the oscillator was considerably decreased by using a 500μfd grid leak capacitor (C19) rather than the 10μfd capacitor called for. In either case there was a tendency for "blocking" of the oscillations to occur. This was overcome by decreasing the capacitance of the grid to plate feedback capacitors C_{15} and C_{18} to the smallest value which would support oscillations. The value required depends on the tank coil used and varies from 10 to 100$\mu\mu$fd.

This oscillator has been found to be extremely sensitive to random noise pulses from radiation and the power lines. In an attempt to completely electrostatically shield the oscillator from radiation noise, it is being constructed in a 3/8 in. brass box of inside dimensions 10x8x3$^{1}/_{4}$ in. This thickness of brass is being used to insure mechanical rigidity in an attempt to achieve high frequency stability in the oscillator. The 100$\mu\mu$fd split stator tank circuit tuning capacitor C_{12} and C_{13} has been submersed in butyl sebacate oil for this same purpose*. The detector and preamplifier will also be housed in the box. In order to prevent power line noise from

*As recommended by Mr. J. G. Bayley of the Chalk River Laboratories

reaching these circuits a power transformer is used in the regulated voltage supply which has electrostatic shielding between the primary and secondary windings.

(7) The Preamplifier

The "400" cycle narrow band amplifier has a 19,000 ohm input impedance. A low impedance load connected to the detector output causes a loading of the oscillator which decreases its sensitivity as a detector of the proton resonance. Furthermore it is desirable to be able to observe the proton resonance peak on an oscilloscope. The output from the diode detector is not sufficiently large to permit this. For these reasons a two stage preamplifier has been constructed. The preamplifier, shown in figure 11, uses a 12SH7 pentode as a voltage amplifier and a 12J5 cathode follower. This circuit provides a gain of 300 and operates from a 180 volt supply.

In order to prevent a 60 cycle ripple from appearing at the preamplifier output it is necessary to operate the filaments of the oscillator, detector, and preamplifier tubes from a d.c. source. In the experimental work this was done by running the tubes, all of which had 6 volt filaments, from a storage battery. The circuits of figures 10 and 11 use tubes whose filaments require 150 milliamperes at 12 volts. These filaments are connected in series along with a suitable dropping resistor and run from the high voltage regulated supply.

(8) The Phase Sensitive Detector

The phase detector shown in figure 15 is the one used by Thomas[24]. While this circuit provides no amplification it does provide d.c. isolation of the control tube circuit from those preceding it and has been chosen for this reason.

(9) The Anti-hunt Circuit

The use of 390 cycle field modulation makes it possible for the proton resonance field discriminator to compensate only for those effects which would otherwise produce slow changes in the magnetic field strength. To compensate for those effects which would otherwise produce rapid changes some other method must be used. Several feedback networks which provide an output proportional to the time rate of change of current through the magnet coil have been tried. An attempt to use the magnet as a transformer in orderto obtain the feedback voltage was unsuccessful. The large distributed capacitance of the magnet coil introduced phase shifts which resulted in the current induced in the secondary coil being less than 90° out of phase with the current through the primary coil at frequencies above 200 cycles. Use of a reference resistor and resistance capacitance coupling was then tried and found to be satisfactory.

The circuit used is shown in figure 15. The 6AC7 amplifier has a gain of 155 over the frequency range from 14,500 to less than 20 cycles per second. The high gain at low frequencies results from the use of 10 μfd coupling condensers. The effect of the feedback loop is to greatly lengthen the time constant of the magnet and this makes the search for the proton resonance very tedious. To eliminate this undesirable behaviour two separate input circuits are provided in the feedback loop. Use of the 0.1 μfd input capacitor (C_{28}) results in a decreased gain in the loop at low frequencies permitting a more rapid change in the magnet current. The switching arrangement shown will make it possible to increase the low frequency gain of the feedback loop before applying the proton resonance signal to the phase detector. Experiments have shown

that unless this sequence is followed regulation does not occur.

(10) The Control Tubes

Because of their low voltage drop and because they do not require a screen voltage supply 6B4G power triodes were tried as the current controlling tubes. The low gain of these tubes when operating with the large impedance of the magnet coil as plate load makes them unsuitable. However 807 power pentodes proved to have a gain some 35 times greater and are shown in figure 15. A Helipot providing fine adjustment of the control tube bias (R_{44}) is necessary in order that the magnetic field strength can be adjusted to the resonance value.

(11) The Magnet Current Power Supply

This is a full wave rectifier circuit using 872-A mercury vapour rectifiers and a two section choke input filter. Its circuit is shown in figure 18. The maximum output is 1 ampere at 1550 volts. The high voltage transformer is connected to its own 2 KW Sola constant voltage transformer through a variac which makes it possible to adjust to a suitable value the voltage drop across the 807 control tubes.

Conclusion

Quantitative measurements of the operation of the regulator cannot be made as yet. The output signal pulses produced by noise pick up in the experimental detector circuit were considerably greater than the proton resonance signal and often a single noise pulse disturbed the control circuit sufficiently to stop regulation. The resultant instability made quantitative measurements impractical. Experiments showed that noise pulses from the power lines were entering the proton resonance detector circuit through the laboratory type audio oscillator being used to provide

the field modulation and the preamplifier power supply leads. To overcome this noise problem necessitated constructing a suitable field modulator and power supply and reconstructing the proton resonance detector and preamplifier. On completion of this construction work quantitative tests of the regulator will be possible.

References

(1) H. E. Duckworth, Rev. Sci. Instr. 21, 54-59 (1950)

(2) P. Preiswerk and P. Stähelin, Helvetica Physica Acta 24, 300-301 (1951)

(3) R. Sagane, S. Kojima, C. Miyamoto, M. Ikawa, Phys. Math. Japan, Proc. 22, 174 (1940)

(4) D. N. Kundu and M. L. Pool, Phys. Rev. 71, 140 (1947)

(5) R. Sher, J. Halpern and A. K. Mann, Phys. Rev. 84, 387 (1951)

(6) J. A. Harvey, Phys. Rev. 81, 353 (1951)

(7) G. E. Boyd and Q. V. Larson, ORNL - 685 (1950)

(8) E. P. Steinberg and L. E. Glendenin, Phys. Rev. 78, 624 (1950)

(9) J. P. Blaser, F. Boehm, P. Marmier and P. Scherrer, Helvetica Physica Acta 24, 441-464 (1951)

(10) Nuclear Data, National Bureau of Standards Circular 499, 100

(11) R. E. Hein, C. M. Fowler, and R. R. McFarlane, Phys. Rev. 85, 138 (1952)

(12) K. Skure, MIT Progress Report May 1951 for the gamma energies and the β^- end point of reference (2)

(13) M. L. Pool, Private communication

(14) D. Kurath, Phys. Rev. 87, 528 (1952), B. Hammermesh, V. Hummel, L. Goodman and D. Engelkemeir, Phys. Rev. 87, 528-529 (1932)

(15) J. A. McCarthy Private communication, Aug. 10, 1952

(16) H. Medicus, P. Preiswerk and P. Scherrer, Helvetica Physica Acta 23 299 (1950)

(17) H. Medicus, A. Mukerji, P. Preiswork, G. de Saussure Phys. Rev. 74, 839 (1948)

(18) J. E. Edwards, M. L. Pool, Phys. Rev. 72, 384 (1947)

(19) N. Metropolis and G. Reitwiesner, Table of Atomic Masses ANL March 1950

(20) S. Geschwind, M. Minden and C. H. Townes, Phys. Rev. 78, 174 (1950) and S. Geschwind and R. Gunther-Mohr, Phys. Rev. 81, 882 (1951)

(21) R. B. Duffield and J. D. Knight, Phys. Rev. 76, 573 (1949)

(22) J. S. Levinger NNES 9 paper 94, and C. Y. Fau, Phys. Rev. 81 300 (A) (1951)

(23) W. H. Burgus, J. D. Knight and E. J. Prestwood, Phys. Rev. 79 104-107 (1950)

(24) H. A. Thomas , Electronics 25, 1, 114 (1952)

(25) E. M. Purcell, H. C. Torrey, and R. V. Pound, Phys. Rev. 69, 37 (1946)

(26) F. Bloch, W. W. Hansen, and M. Packard, Phys. Rev. 70, 474 (1946)

(27) N. Bloembergen, E. M. Purcell, and R. V. Pound, Phys. Rev. 73, 679 (1948)

(28) H. A. Thomas, R. L. Driscoll and J. A. Hipple, Phys. Rev. 75, 902 (1949)

(29) A. Roberts, Rev. Sci. Inst. 18, 845 (1947)

(30) N. J. Hopkins, Rev. Sci. Inst. 20, 401 (1949)

(31) R. V. Pound and W. D. Knight, Rev. Sci. Inst. 21, 219 (1950)

(32) H. W. Knoebel and E. L. Hahn, Rev. Sci. Inst. 22, 904 (1951)

(33) G. M. Volkoff, H. E. Petch and D. W. L. Smellie, Can. Jr. Res. 30, 270 (1952)

(34) J. R. Zimmerman and D. Williams, Phys. Rev. 73, 94(1948)

LIST OF COMPONENTS

Regulated Power Supply (figure 14)

V1	5U4G
V2	3-6B4G tubes in parallel
V3	12SH7
V4	VR150
T1	HAMMOND Special Transformer #32117
L1	HAMMOND 10-200X choke
L2	HAMMOND 10-200X choke
C1	10 microfarod, 600 volt electrolytic condenser
C2	10 microfarad, 450 volt electrolytic condenser
C3	10 microfarad, 450 volt electrolytic condenser
R1	15,000 ohm, 10 watt w.w.
R2	50,000 ohm potentiometer, w.w.
R3	10,000 ohm, 10 watt w.w.
R4	100,000 ohm, 20 watt w.w.
R5	30,000 ohm, 10 watt w.w.
R6	7,000 ohm, 10 watt w.w.
R7	100,000 ohm, 2 watt carbon
R8	330,000 ohm, 2 watt carbon
R9	750 ohms, 100 watts adjustable w.w.
R10	750 ohms, 100 watts adjustable w.w.

Field Modulator (figure 12)

V5	6SN7
V6	6SN7
VII	VR150
T2	HAMMOND Transformer #331
T3	HAMMOND Transformer #445
C4	0.01 microfarad, 600 volt paper
C5	0.01 microfarad, 600 volt paper
C6	0.1 microfarad, 600 volt paper
C7	50 microfarad, 50 volt electrolytic
C9	0.25 microfarad, 600 volt paper
C10	50 microfarad, 50 volt electrolytic
C11	8 microfarad, 450 volt electrolytic
R11	75,000 ohm, 1 watt carbon
R12	10,000 ohm } ganged potentiometer w.w.
R13	10,000 ohm }
R14	27,000 ohm, 1 watt carbon
R15	22,000 ohm, 2 watt carbon
R16	4.7 megohm, 1/4 watt carbon
R17	1000 ohm, 1 watt carbon
R18	22,000 ohm, 2 watt carbon
R19	100,000 ohm potentiometer w.w.
R20	50,000 ohm, 1/2 watt carbon
R21	100,000 ohm potentiometer w.w.
R22	5,000 ohm, 10 watt w.w.
R23	1,000 ohm, 1 watt carbon
R24	10,000 ohm, 2 watt carbon

Oscillator and Detector (figure 10)

V7	12SC7
V8	12H6
L3	Wound on 3/8 in. diameter form and $1^{1}/4$ in. long: 0.006 milli-henrys
L4	2.5 milli-henry radio-frequency choke
L5	2.5 milli-henry radio-frequency choke
C12, C13	100 micro-microfarad split stator air condenser submersed in butyl sebacate oil
C14	It is proposed to add a variable condenser at a later date which will permit fine adjustment of the oscillator frequency.
C15	See page 21
C16	100 micro-microfarad ceramic
C17	100 micro-microfarad ceramic
C18	See page 21
C19	500 microfarad, 6 volt electrolytic
C20	100 micro-microfarad ceramic
C21	0.005 microfarad, 600 volt paper
C22	10,000 micro-microfarad ceramic
R25	100,000 ohm, 1/2 watt carbon
R26	100,000 ohm, 1/2 watt carbon
R27	1 megohm and 2.2 megohm, 1/2 watt carbon resistors in series
R28	100,000 ohm, 1/2 watt carbon
R29	50,000 ohm potentiometer w.w.
R30	100,000 ohm, 1/2 watt carbon
R31	100,000 ohm, 1 watt carbon
R32	100,000 ohm, 1/2 watt carbon
R33	1 megohm, 1/2 watt carbon
R34	27,000 ohm, 1/2 watt carbon

Preamplifier (figure 11)

V9	12SH7
V10	12J5GT
C23	24 microfarad, 150 volt electrolytic
C24	0.1 microfarad, 600 volt paper
C25	0.005 microfarad, 600 volt paper
C26	1 microfarad, 250 volt paper
C27	0.05 microfarad, 600 volt paper
R35	3,300 ohm, 1 watt carbon
R36	1 megohm, 1/2 watt carbon
R37	470,000 ohm, 1 watt carbon
R38	1 megohm, 1/2 watt carbon
R39	1,200 ohm, 1 watt carbon
R40	180,000 ohm, 1/2 watt carbon
R41	22,000 ohm, 1 watt carbon

Phase Detector, Control Tube and Anti-Hunt Circuits (figure 15)

V11	807
V12	807 Two tubes used with test magnet. Ten tubes in parallel will be required for the completed unit.
V13	6AC7
T4	HAMMOND Transformer #331
D_1	IN34 crystal diode
D_2	IN34 crystal diode
B1	45 volt battery
C28	0.1 microfarad, 600 volt paper
C29	10 microfarad, 600 volt oil-filled
C30	500 microfarad, 6 volt electrolytic

C31	10 microfarad, 450 volt electrolytic
C32	10 microfarad, 600 volt oil-filled
C33	1 microfarad, 600 volt paper
C34	1 microfarad, 600 volt paper
P42	120,000 ohm, 1/2 watt carbon
P43	20,000 ohm potentiometer w.w.
P44	100,000 ohm HELIPOT (15 turn)
P45	120,000 ohm, 1/2 watt carbon
P46	300 ohm, 10 watt w.w. For use with test magnet.
P47	100 ohm, 1 watt carbon
P48	100 ohm, 1 watt carbon
P49	100,000 ohm, 1/2 watt carbon
P50	180,000 ohm, 1 watt carbon
P51	100,000 ohm, 1/2 watt carbon
P52	100,000 ohm, 1/2 watt carbon
P53	10,000 ohm, 1 watt and 1,000 ohm, 1 watt carbon resistors in parallel

Magnet Current Power Supply (figure 18)

V14	8 72-A
V15	8 72-A
T5	HAMMOND Transformer #1172T
T6	HAMMOND Transformer #779
L6	HAMMOND 10V1000 choke
L7	HAMMOND 10V1000 choke
T.D.R.	GUARDIAN time delay relay

Variac	110 volts, 20 amperes, 60 cycles
C34	10 microfarad, 1500 volt oil-filled
C35	10 microfarad, 1500 volt oil-filled
R34	7 - 10,000 ohm, 10 watt w.w. resistors in series.

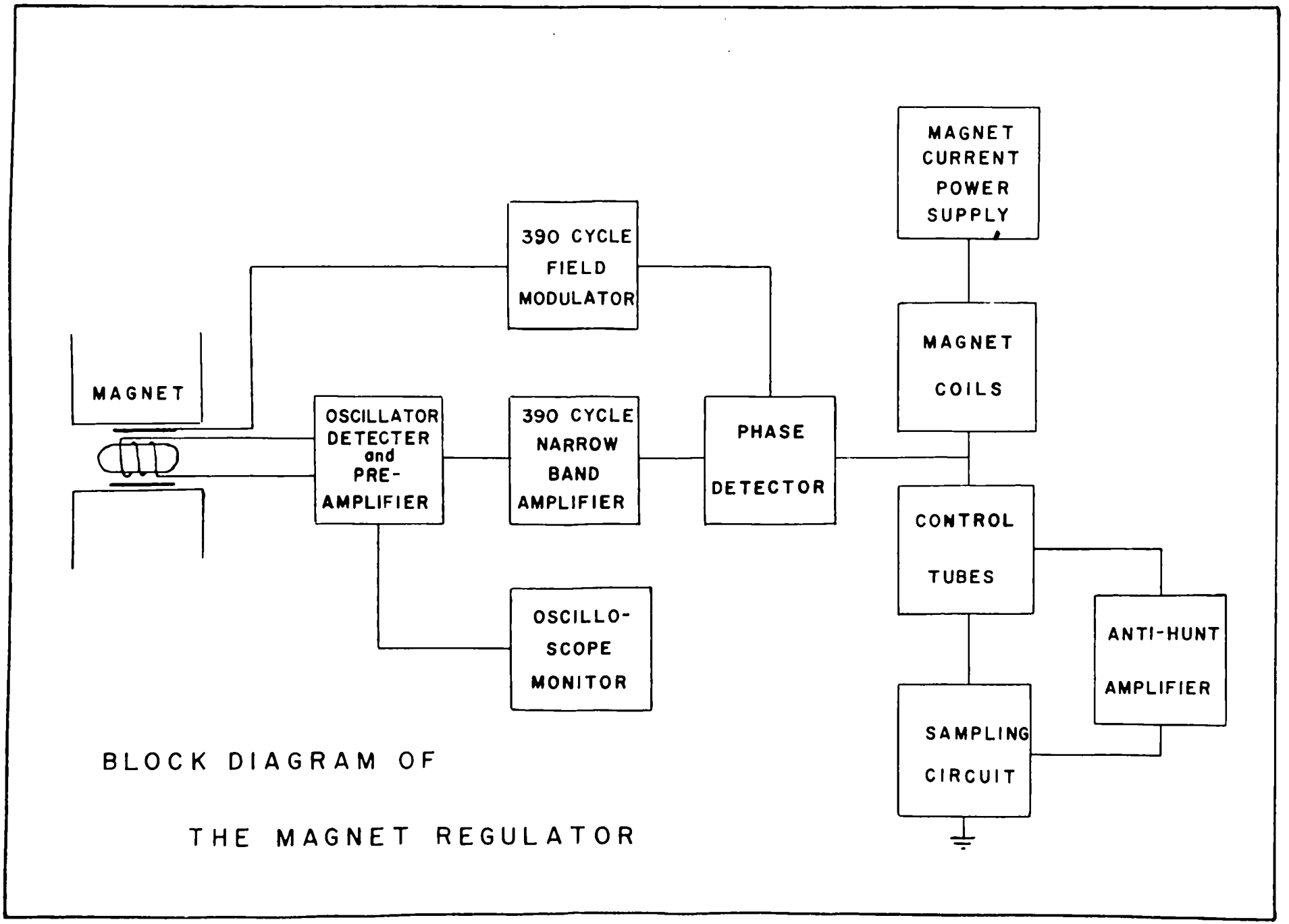
MAGNET CURRENT POWER SUPPLY
390 CYCLE FIELD MODULATOR
MAGNET
MAGNET COILS
OSCILLATOR DETECTER and PRE-AMPLIFIER
390 CYCLE NARROW BAND AMPLIFIER
PHASE DETECTOR
CONTROL TUBES
OSCILLO-SCOPE MONITOR
ANTI-HUNT AMPLIFIER
SAMPLING CIRCUIT
BLOCK DIAGRAM OF
THE MAGNET REGULATOR

FIGURE 9

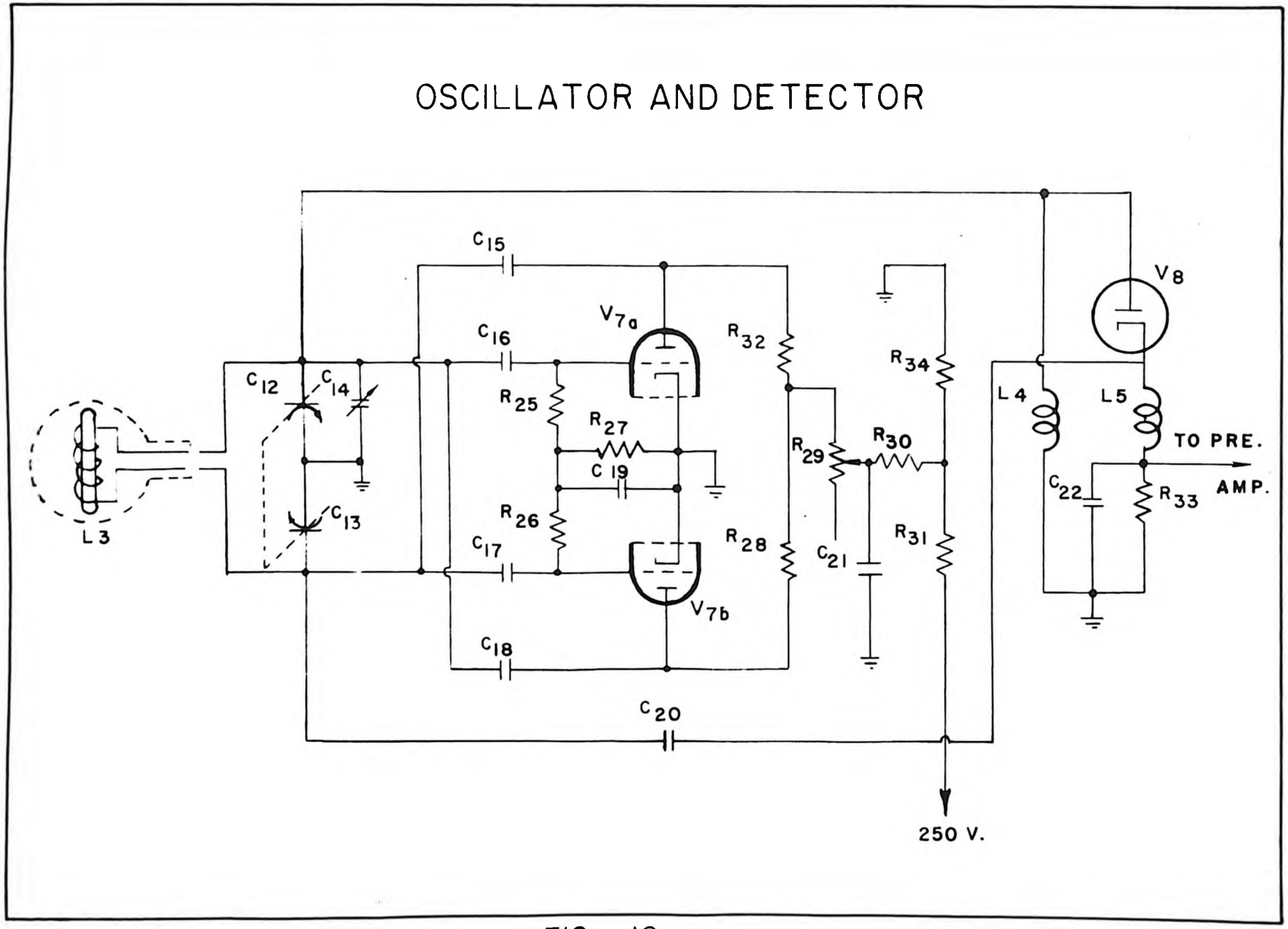
OSCILLATOR AND DETECTOR
C15
C16
C12
C14
C13
L3
V7a
V7b
R25
R27
C19
R26
C17
C18
R32
R34
R29
R30
R28
C21
R31
C20
250 V.
V8
L4
L5
TO PRE.
AMP.
C22
R33

FIG 10

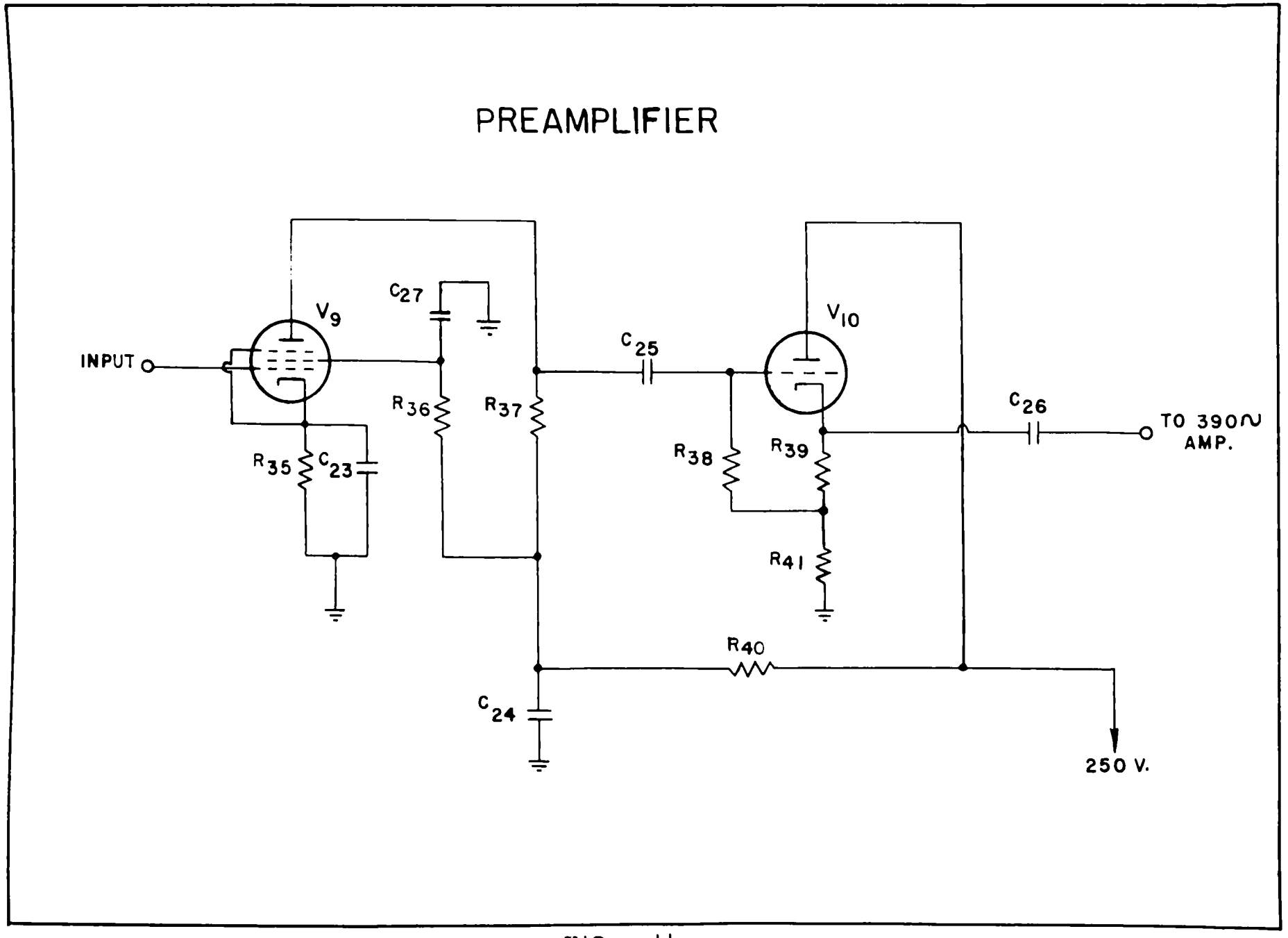
PREAMPLIFIER
INPUT
V9
C27
R36
R37
C25
V10
C26
TO 390Ω AMP.
R35
C23
R38
R39
R41
R40
C24
250 V.

FIG 11

FIELD MODULATOR

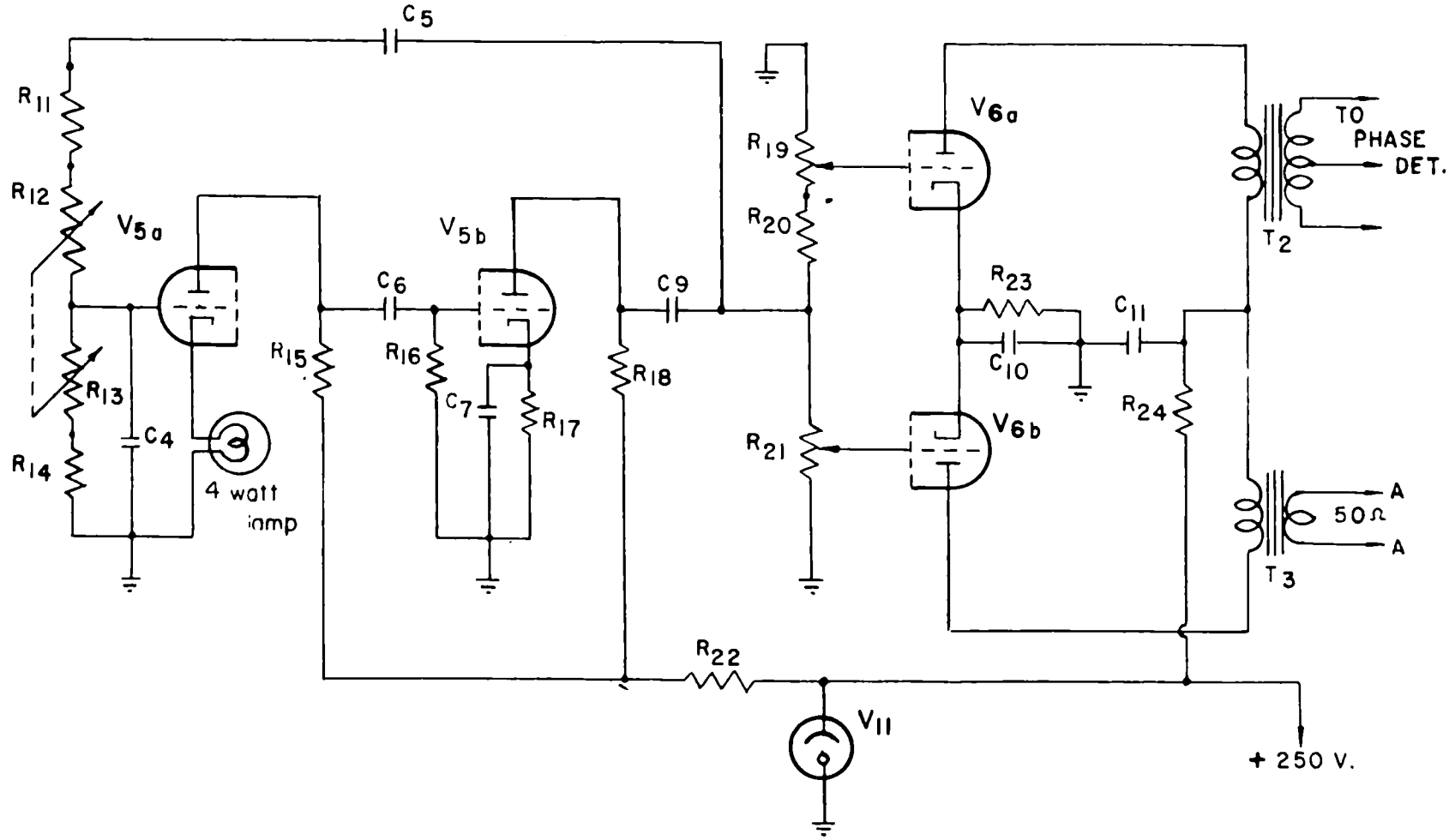

FIGURE 12

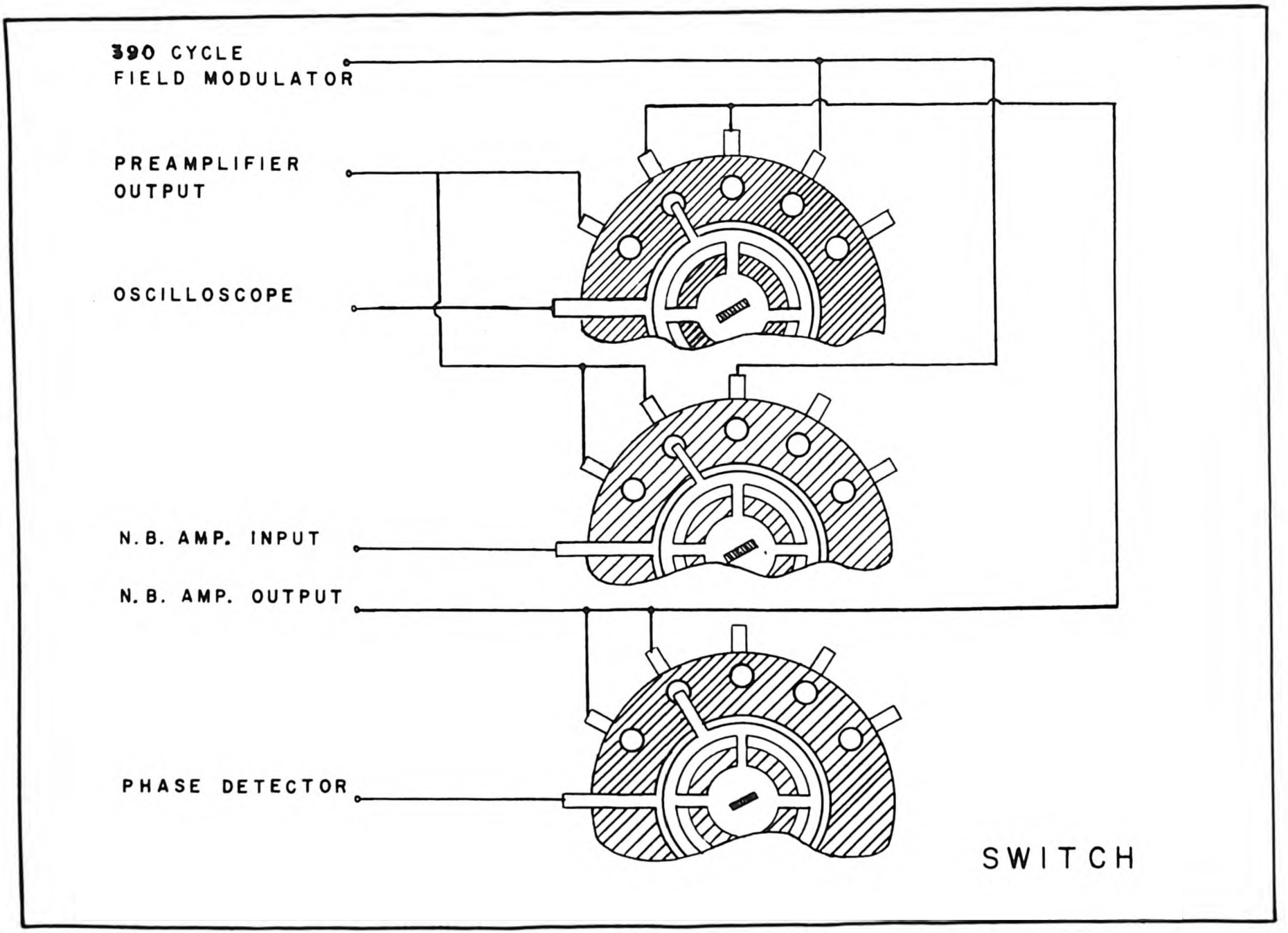
390 CYCLE
FIELD MODULATOR
PREAMPLIFIER
OUTPUT
OSCILLOSCOPE
N.B. AMP. INPUT
N.B. AMP. OUTPUT
PHASE DETECTOR
SWITCH

FIGURE 13

REGULATED POWER SUPPLY

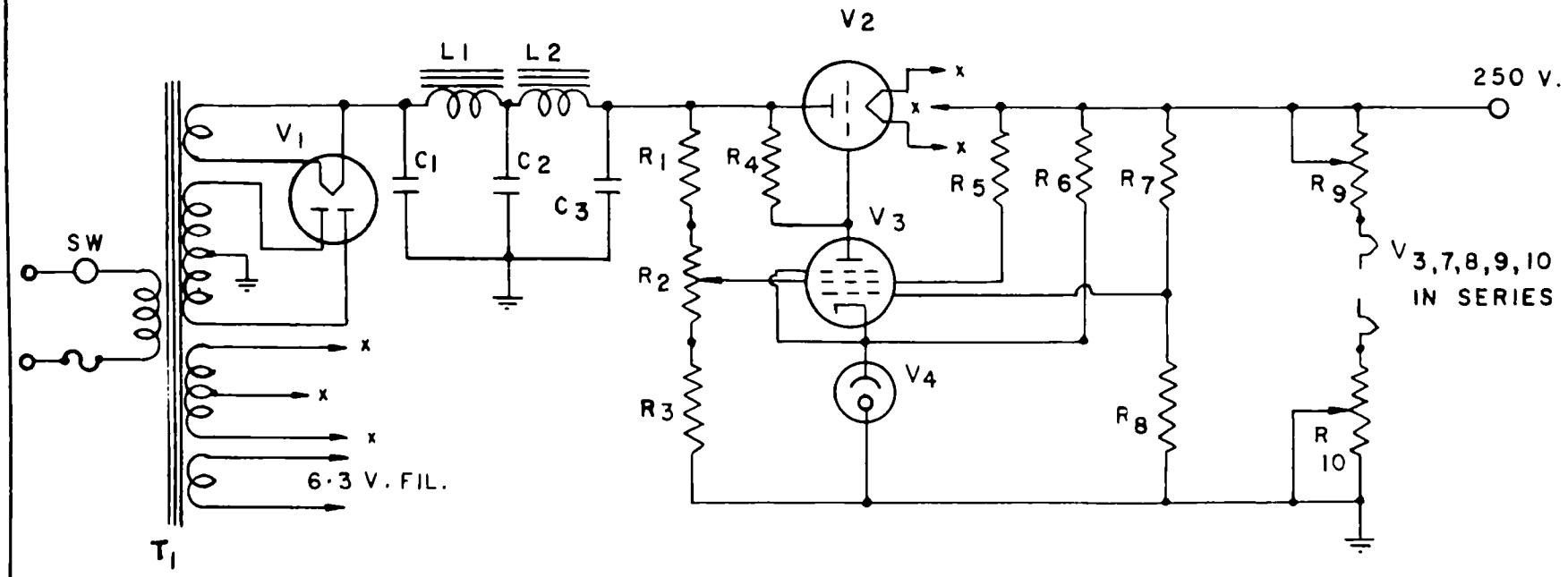

FIG. 14

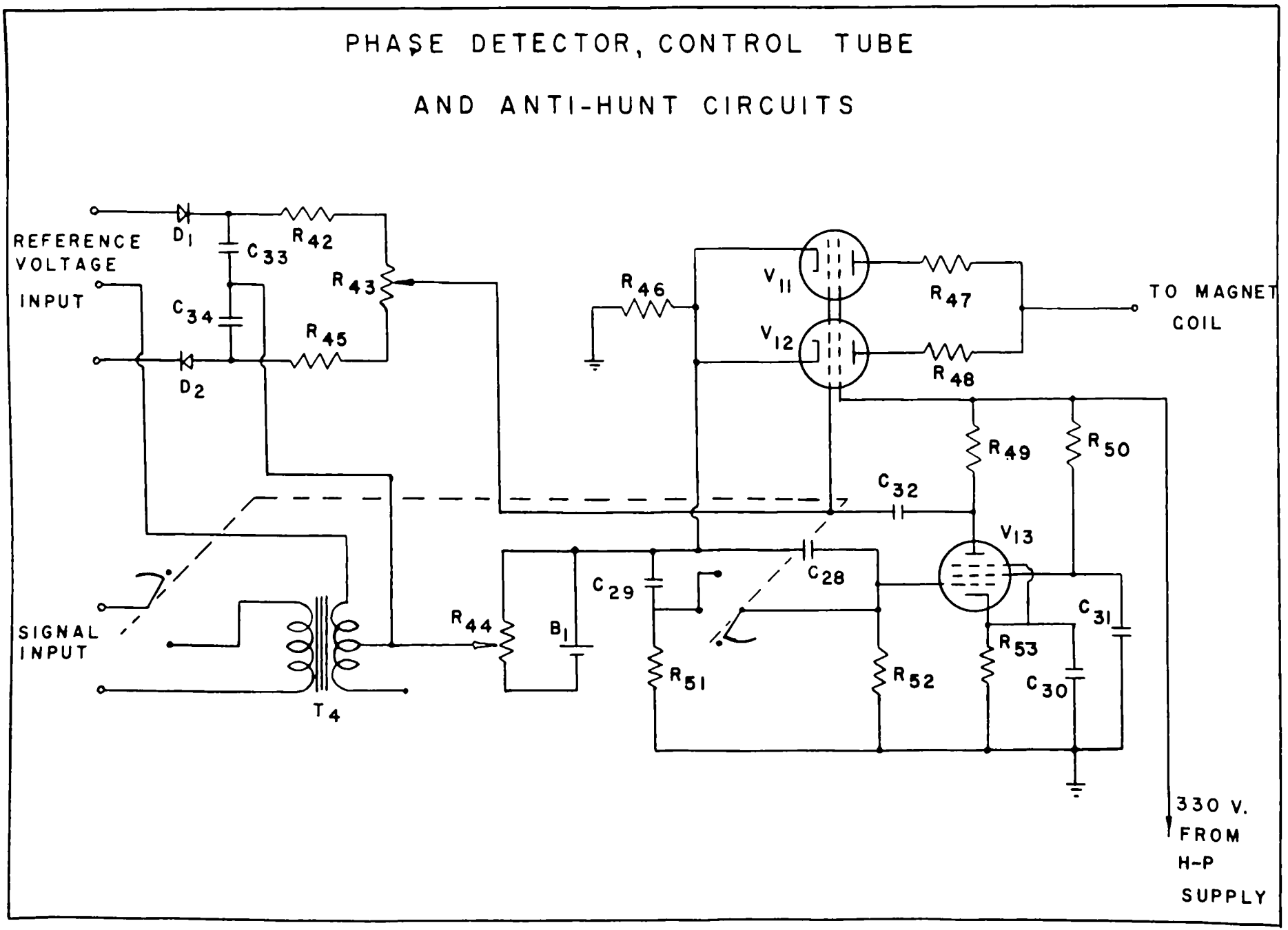
PHASE DETECTOR, CONTROL TUBE
AND ANTI-HUNT CIRCUITS
REFERENCE VOLTAGE INPUT
D1
C33
R42
R43
C34
R45
D2
R46
V11
V12
R47
R48
TO MAGNET COIL
R49
R50
C32
V13
C29
C28
C31
SIGNAL INPUT
R44
B1
R51
R52
R53
C30
T4
330 V. FROM H-P SUPPLY

FIGURE 15

PROBE

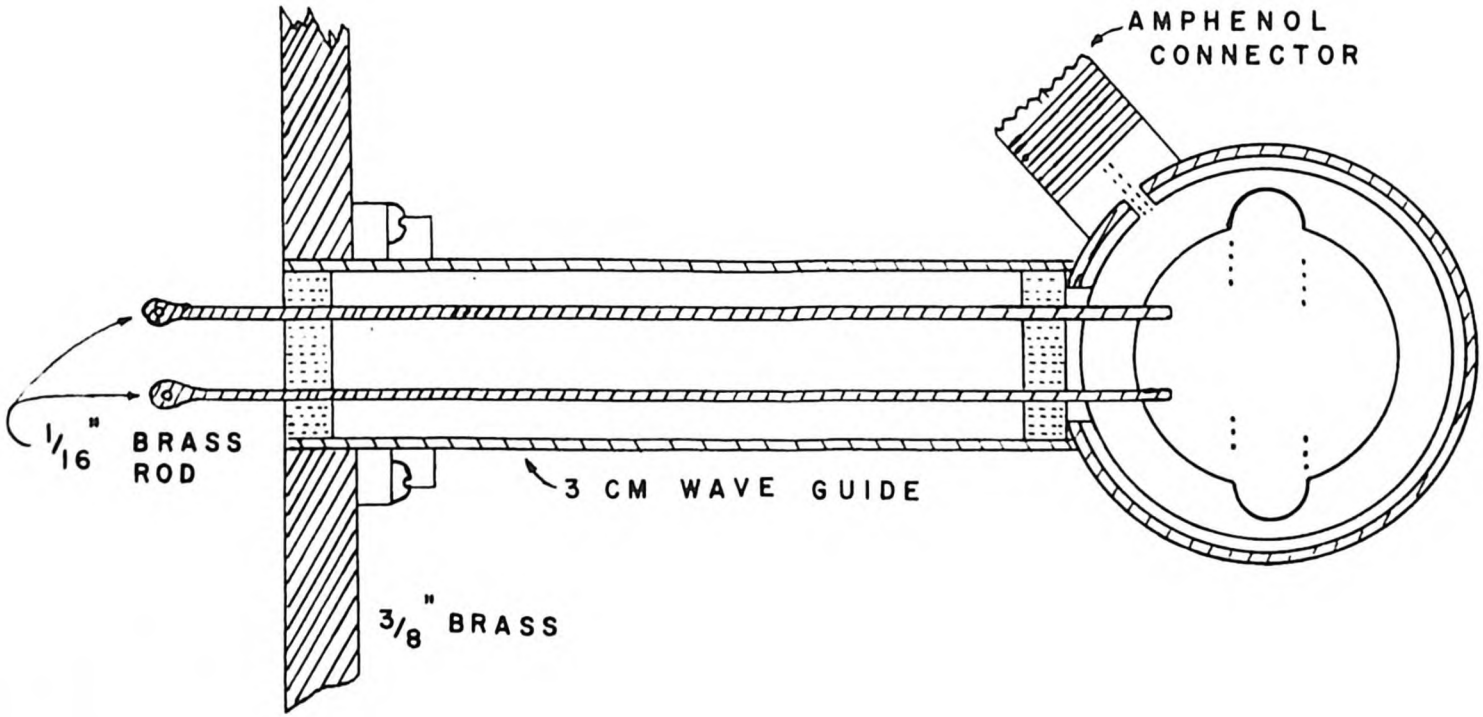

FIGURE 16

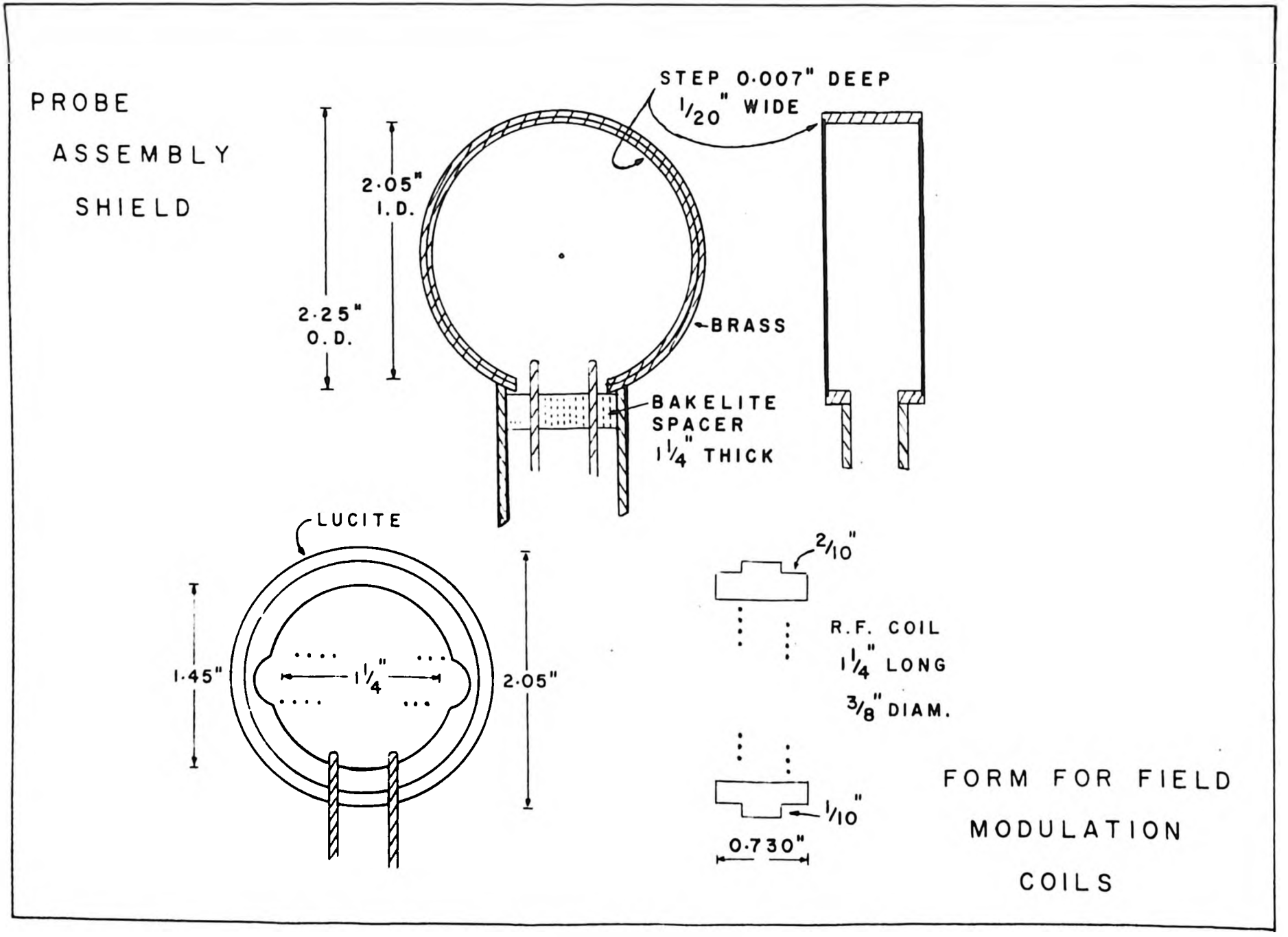
PROBE
ASSEMBLY
SHIELD
STEP 0.007" DEEP
1/20" WIDE
2.05"
I.D.
2.25"
O.D.
BRASS
BAKELITE
SPACER
1 1/4" THICK
LUCITE
1.45"
1 1/4"
2.05"
2/10"
R.F. COIL
1 1/4" LONG
3/8" DIAM.
1/10"
0.730"
FORM FOR FIELD
MODULATION
COILS

FIGURE 17

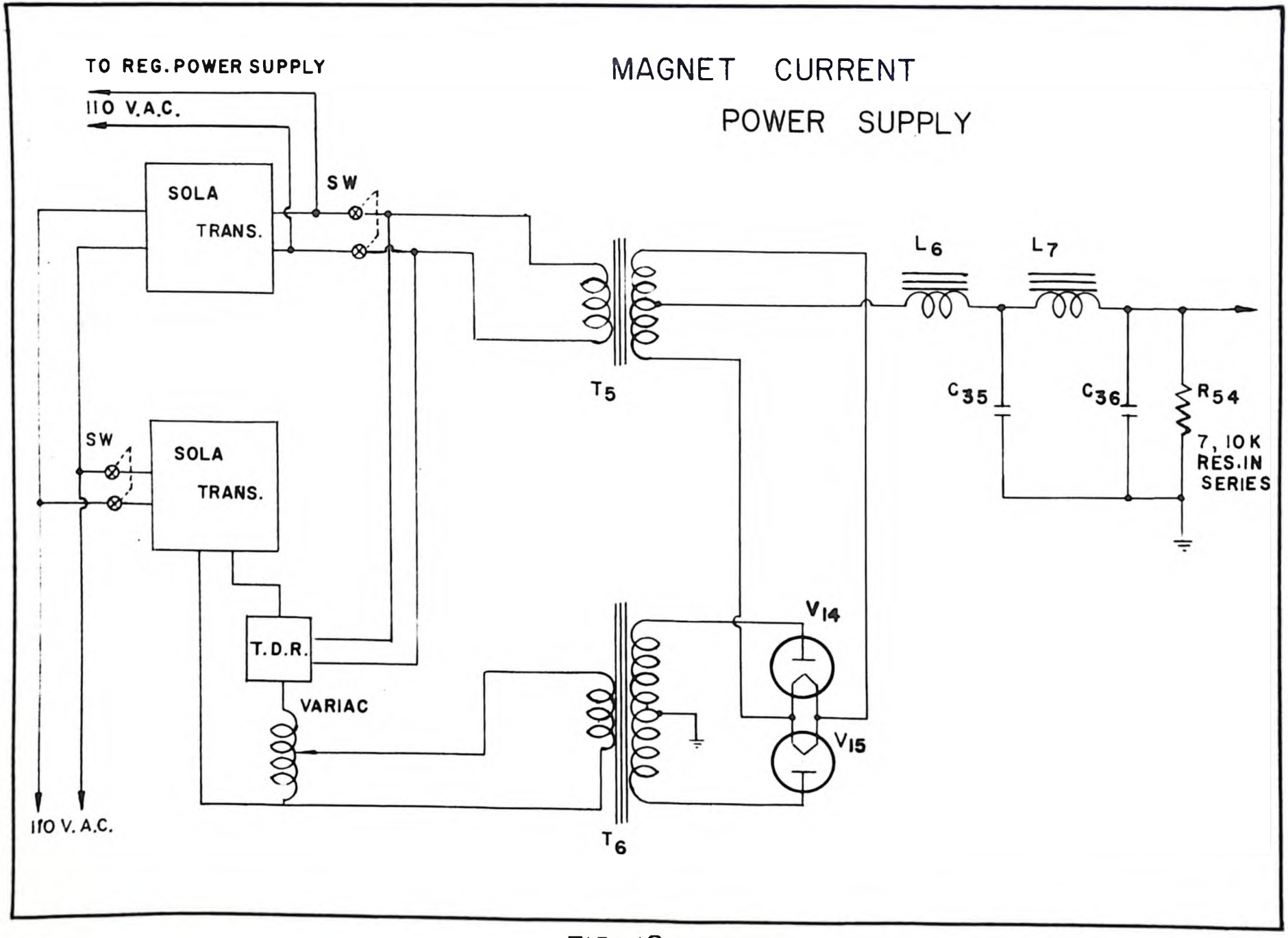
MAGNET CURRENT
POWER SUPPLY
TO REG. POWER SUPPLY
110 V.A.C.
SOLA
TRANS.
SW
SW
SOLA
TRANS.
T.D.R.
VARIAC
110 V. A.C.
T5
T6
L6
L7
C35
C36
R54
7, 10K
RES. IN
SERIES
V14
V15

FIG. 18